Preparation, Crystal and Magnetic Structure, and Magnetotransport Properties of the Double Perovskite $CaCu_{2.5}Mn_{4.5}O_{12}$

J. Sánchez-Benítez,[†] J. A. Alonso,*[,†] M. J. Martínez-Lope,[†] M. T. Casais,[†] J. L. Martínez,[†] A. de Andrés,[†] and M. T. Fernández-Díaz[‡]

Instituto de Ciencia de Materiales de Madrid, CSIC, Cantoblanco, E-28049 Madrid, Spain, and Institut Laue-Langevin, B.P. 156, F-38042 Grenoble Cedex 9, France

Received July 17, 2002. Revised Manuscript Received March 10, 2003

$CaCu_{2.5}Mn_{4.5}O_{12}$ perovskite has been prepared in polycrystalline form under moderate pressure conditions of 20 kbar, in the presence of $KClO_4$ as oxidizing agent. This material has been studied by X-ray and neutron powder diffraction (NPD), magnetic, magnetotransport, and thermopower measurements. The crystal structure is cubic, space group $Im\bar{3}$ (No. 204), with $a = 7.2279(1)$ Å at room temperature (RT). In the ABO_3 perovskite superstructure, the A positions are occupied by Ca^{2+} and ($Cu_{2.5}{}^{2+}Mn_{0.5}{}^{3+}$), ordered in a 1:3 arrangement giving rise to the body-centering of the unit cell. At the B positions, Mn adopts a mixed oxidation state of 3.875+; MnO_6 octahedra are considerably tilted by 19°, due to the relatively small size of the A-type cations. The Curie temperature is 345 K. Low temperature (2 K) NPD data show evidence for a ferrimagnetic coupling between $Mn^{3.875+}$ and ($Cu_{2.5}{}^{2+}Mn_{0.5}{}^{3+}$) spins, with ordered magnetic moments of 2.32(5) and −0.54(3) μ_B, respectively. An additional canting effect of the Mn moments at B positions has been detected below 70 K, breaking down the body centered symmetry. We have developed a microscopic model that explains both the saturation magnetization values and the refined magnetic moments at A and B positions. Our results show that Cu^{2+} and Mn^{3+} spins at the A substructure are almost perpendicular to each other. A magnetoresistance (MR) of 34% has been observed at 5 K for $\boldsymbol{H} = 9$ T; the low field MR at RT is as high as 2% and shows an appreciable temperature stability.

Introduction

Materials exhibiting colossal magnetoresistance (CMR) undergo a large change in electrical resistance in response to an external magnetic field. This effect is of technological interest as it can be used for the detection of magnetic fields in magnetic memory devices. A range of compounds has now been found to exhibit intrinsic CMR;[1,2] most of them are manganese perovskites based on $LaMnO_3$, in which extra charge carriers (holes) are introduced by chemical substitution of alkaline-earth cations for La. In the attractive field of the CMR oxides, considerable effort is still needed before their practical applications can be found, mainly because the CMR response at low field and room temperature is negligible in the best known systems (the mentioned rare-earth−manganese perovskites), or other more exotic phases such as the $Tl_2Mn_2O_7$ pyrochlore or iron double perovskites. Recently, a "new" system has attracted the attention of the CMR community: the complex perovskite $CaCu_3Mn_4O_{12}$.[3−6] This ferromagnetic oxide (T_C = 355 K) shows good low-field response, as large as 40% at 20 K, and this response does not show the strong temperature-dependent decay characteristic of other perovskite-based systems.

In fact, this compound had already been described in the 1970s, when the preparation and crystal structure of some related phases were reported.[7−9] The crystal structure of $CaCu_3Mn_4O_{12}$ has the originality of containing Cu^{2+} (or other Jahn−Teller transition metal cations, such as Mn^{3+}) at the A positions of the ABO_3 perovskite; this Jahn−Teller cation and Ca^{2+} are 1:3 ordered in a $2\mathbf{a_0} \times 2\mathbf{a_0} \times 2\mathbf{a_0}$ cubic cell of $Im\bar{3}$ symmetry (where $\mathbf{a_0}$ is a unit cell of the perovskite aristotype). This material, and other compounds of the $A'A_3B_4O_{12}$ family, have been prepared under high pressure (70 kbar), necessary to stabilize the small A cations in the twelvefold positions of the perovskite.

* To whom correspondence should be addressed. Phone: +34-91-334-9071. Fax: +34-91-372-0623. E-mail: ja.alonso@icmm.csic.es.
[†] Instituto de Ciencia de Materiales de Madrid, CSIC.
[‡] Institut Laue-Langevin.

(1) Ramirez, A. P. *J. Phys: Condens. Matter* **1997**, *9*, 8171.
(2) Rao, C. N. R., Raveau, B., Eds. Colossal Magnetoresistance and Other Related Properties in 3d Oxides; World Scientific: Singapore, 1998.
(3) Zeng, Z.; Greenblatt, M.; Subramanian, M. A.; Croft, M. *Phys. Rev. Lett.* **1999**, *82*, 3164.
(4) Wu, H.; Zheng, Q.; Gong, X. *Phys. Rev. B* **2000**, *61*, 5217.
(5) Weht, R.; Pickett, W. E. *Phys. Rev. B* **2001**, *65*, 14415.
(6) Troyanchuk, I. O.; Lobanovsky, L. S.; Kasper, N. V.; Hervieu, M.; Maignan, A.; Michel, C.; Szymczak, H.; Szewczyk, A. *Phys. Rev. B* **1998**, *58*, 14903.
(7) Chenavas, J.; Joubert, J. C.; Marezio, M.; Bochu, B. *J. Solid State Chem.* **1975**, *14*, 25.
(8) Bochu, B.; Chenavas, J.; Joubert, J. C.; Marezio, M. *J. Solid State Chem.* **1974**, *11*, 88.
(9) Marezio, M.; Dernier, P. D,; Chenavas, J.; Joubert, J. C. *J. Solid State Chem.* **1973**, *6*, 16.

10.1021/cm0212616 CCC: $25.00
Published on Web 04/29/2003

We can consider that $CaCu_3Mn_4O_{12}$ is the $x = 0$ term of the $CaCu_{3-x}Mn_{4+x}O_{12}$ series, in which Cu^{2+} cations are progressively replaced by Mn^{3+} at the A substructure of the perovskite. This replacement implies a gradual change of the oxidation state of Mn at the B positions, from 4+ ($x = 0$) to 3.25+ ($x = 3$). For the term of the series with $x = 3$, $CaMn_7O_{12}$, a trigonal symmetry was described from an XRD single crystal study, where the oxygen positions were only approximately determined.[8] For the intermediate members ($0 \leq x \leq 2$) the crystal structure has not yet been reported. The mixed nominal valence of Mn (at B positions) in these intermediate compounds allows one to predict interesting electronic effects, such as double exchange, charge disproportionation, or charge ordering. For instance, charge-ordering phenomena have been described to occur at 180 K for the related $NaMn_7O_{12}$[9] oxide (with nominal $Mn^{3.5+}$ at the B substructure).

Recently, Zeng et al.[10] have described the magnetic and magnetotransport properties of the series $CaCu_{3-x}Mn_{4+x}O_{12}$, prepared under 180 bar of oxygen pressure and moderate temperatures of 700 °C. A related compound, with stoichiometry $Na_{0.5}Ca_{0.5}Cu_{2.5}Mn_{4.5}O_{12}$, was also reported to show magnetotransport properties similar to those of $CaCu_{2.5}Mn_{4.5}O_{12}$.[11] However, a microscopic description of the magnetism in the $0 \leq x \leq 1$ range was still lacking. Recently, we have been able to prepare $CaCu_{2.5}Mn_{4.5}O_{12}$ at moderate pressures of 20 kbar, in the presence of $KClO_4$ as oxidizing agent. This alternative preparation procedure allowed us to obtain well-crystallized samples, suitable to perform an accurate neutron diffraction study of both structure and magnetism. Low-temperature NPD data allowed us to probe the microscopic origin of the magnetic ordering, concerning both $(Cu_{2.5}{}^{2+}Mn_{0.5}{}^{3+})_A$ and $(Mn_4{}^{3.875+})_B$ magnetic substructures. The magnetic and magnetotransport properties are also discussed at the light of the NPD data.

Experimental Section

The elaboration of $CaCu_{2.5}Mn_{4.5}O_{12}$ required the previous preparation of very reactive precursors, obtained by wet-chemistry techniques. A mixture of $CaCO_3$, $Cu(NO_3)_2{\cdot}3H_2O$, and $MnCO_3$ was dissolved in citric acid; the solution was slowly evaporated, leading to an organic resin which was dried at 120 °C and slowly decomposed at temperatures up to 600 °C. The sample was then heated at 800 °C for 2 h to eliminate all the organic materials and nitrates. This precursor was thoroughly ground with $KClO_4$ (30% in weight), put into a gold capsule (8 mm diameter, 10 mm length), sealed, and placed in a cylindrical graphite heater. The reaction was carried out in a piston-cylinder press (Rockland Research Co.), at a pressure of 2 GPa at 1000 °C for 60 min. Then the material was quenched to room temperature and the pressure was subsequently released. A fraction of the raw product, obtained as a dense, homogeneous pellet, was partially ground to perform the structural and magnetic characterization; some as-grown pellets were kept for magnetotransport measurements. The ground product was washed in a dilute HNO_3 aqueous solution to dissolve KCl coming from the decomposition of $KClO_4$ and to eliminate small amounts of unreacted CuO; then the powder sample was dried in air at 150 °C for 1 h.

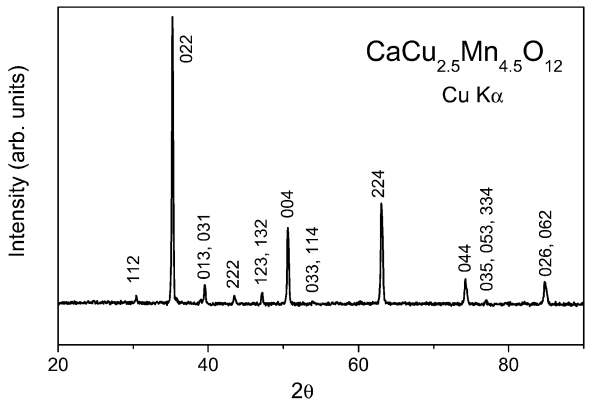

Figure 1. XRD pattern for $CaCu_{2.5}Mn_{4.5}O_{12}$ indexed in a cubic unit cell with $a = 7.2279(1)$ Å.

The product was initially characterized by laboratory XRD (Cu Kα, $\lambda = 1.5406$ Å) for phase identification and to assess phase purity. For the structural refinements, NPD patterns were collected at room temperature and at 2 K at the high resolution D2B neutron diffractometer of ILL-Grenoble. Despite the relatively small amount of sample available (about 1 g), a good quality pattern could be collected with the high-flux mode and a counting time of 4 h for each pattern. A wavelength of 1.594 Å was selected from a Ge monochromator. High-temperature medium-resolution NPD patterns were collected at the D1B diffractometer to follow the thermal evolution of the ferromagnetic component. The sample was placed in a standard orange cryostat and cooled to 1.5 K; then sequential NPD diagrams were collected during the heating run, at 1.3 K min^{-1}, in the 1.5−315 K temperature range, with a counting time of 15 min per diagram. All the patterns were refined by the Rietveld method, using the FULLPROF refinement program.[12] A pseudo-Voigt function was chosen to generate the line shape of the diffraction peaks. No regions were excluded in the refinement. In the final run the following parameters were refined from the high-resolution D2B data: scale factor, background coefficients, zero-point error, unit-cell parameters, pseudo-Voigt corrected for asymmetry parameters, positional coordinates, isotropic thermal factors, and magnitude of the Cu and Mn magnetic moments. The coherent scattering lengths for Ca, Cu, Mn, and O were 4.70, 7.718, −3.73, and 5.803 fm, respectively. The magnetic form factors considered for Cu and Mn cations were determined with the coefficients taken from the International Tables of Crystallography.

The dc and ac magnetic susceptibility was measured with a commercial SQUID magnetometer on powdered samples, in the temperature range 5−720 K; transport and magnetotransport measurements were performed by the conventional four-probe technique, under magnetic fields up to 9 T in a PPMS system from Quantum Design.

Results

$CaCu_{2.5}Mn_{4.5}O_{12}$ was obtained as a black, well-crystallized powder. It is worth commenting that the synthesis procedure used in this work is complementary to that previously described[10] in the sense that it allowed us to obtain very well-crystallized and oxygen-stoichiometric samples, suitable to perform the diffraction experiments which are the main aim of this report. Trials to work at lower temperatures, as the reported 700° C,[10] led to inferior quality samples as far as the crystallization is concerned. The laboratory XRD diagram is shown in Figure 1. The pattern is characteristic of a cubic perovskite showing sharp, well-defined su-

(10) Zeng, Z.; Greenblatt, M.; Sunstrom, J. E.; Croft, M.; Khalid, S. *J. Solid State Chem.* **1999**, *147*, 185.
(11) Zeng, Z.; Greenblatt, M.; Croft, M. *Phys. Rev. B* **1998**, *58*, R595.
(12) Rodríguez-Carvajal, J. *Physica B (Amsterdam)* **1993**, *192*, 55.

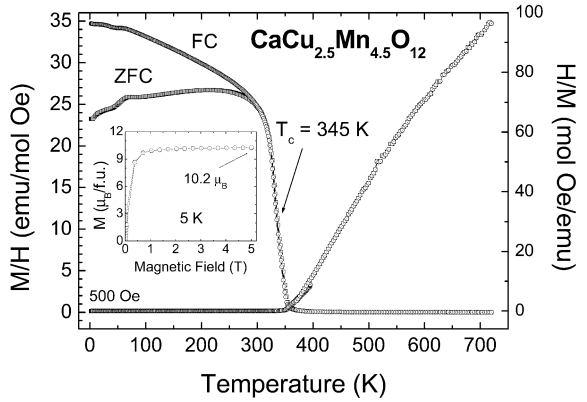

Figure 2. Temperature dependence of the dc magnetic susceptibility (FC and ZFC) and reciprocal susceptibility (right axis). The inset shows the magnetization vs magnetic field plot at 5 K of $CaCu_{2.5}Mn_{4.5}O_{12}$.

perstructure reflections due to the 1:3 ordering of Ca and ($Cu_{2.5}Mn_{0.5}$) cations. No impurity phases were detected from either XRD or NPD data.

Magnetic Data. The magnetization vs temperature data (Figure 2) shows a saturation characteristic of the spontaneous ferromagnetic ordering described earlier[3] for the parent perovskite $CaCu_3Mn_4O_{12}$. The inflection in the magnetization at 345 K, labeled as T_C in Figure 2, is slightly lower than the reported Curie temperature for $CaCu_3Mn_4O_{12}$, of 355 K.[3] There is a large difference between zero-field-cooled (ZFC) and field-cooled (FC) curves, suggesting the presence of irreversibility processes or the possibility of canting of the magnetic moments. The ZFC curve shows an anomaly (small susceptibility peak) at 63 K, the origin of which can be understood in light of the neutron results, as will be commented later. In a previous work on $CaCu_{2.5}Mn_{4.5}O_{12}$, a T_C of 340 K was reported and the anomaly at 63 K was not described.[10] Above T_C, the reciprocal susceptibility data (right axis of Figure 2) shows a progressive change of slope, which diminishes as temperature increases. This behavior of the reciprocal susceptibility is a typical feature of ferrimagnetic compounds. A fitting to the Curie−Weiss law in the 400−550 K interval gives a paramagnetic effective moment of 5.70 μ_B/formula unit (fu) and a Weiss constant of Θ_W = 360 K; in the 560−720 K range the observed paramagnetic moment is 6.73 μ_B/fu and Θ_W = 282 K. The magnetization vs magnetic field data shown in the inset of Figure 2 at 5 K are characteristic of a ferromagnet with a saturation magnetic moment of 10.2 μ_B/fu.

Structural Refinement. The structural refinement from RT high-resolution NPD data was performed in the $Im\bar{3}$ (No. 204) space group, with a unit-cell parameter related to $\mathbf{a_0}$ (ideal cubic perovskite, $\mathbf{a_0} \approx 3.8$ Å) as $\mathbf{a} \approx 2\mathbf{a}_0$, using the $CaCu_3Mn_4O_{12}$ structure as starting model, with Ca atoms at 2a (0 0 0) positions, Cu at 6b (0 $^1/_2$ $^1/_2$) positions, Mn at 8c ($^1/_4$ $^1/_4$ $^1/_4$), and O at 24*g* (*x y* 0) sites. A reasonable fit ($R_I \approx 8\%$) was obtained for this preliminary model. As a second step, Mn atoms were introduced at random at 6b positions together with Cu, and the complementary occupancy factors were refined, constrained to a full occupancy. After this refinement the quality of the fit was notably improved, reaching a discrepancy factor of R_I = 3.85%. The subsequent refinement of the occupancy factor for oxygen positions gave no significant deviation from the full stoichiometry. The resulting crystallographic formula for this material is $Ca[Cu_{2.46(2)}Mn_{0.54(2)}]_{6b}[Mn_4]_{8c}O_{11.8(1)}$. Assuming a valence of 2+ for Cu cations, and 3+ for Mn at the 6b sublattice, the nominal valence for Mn at 8c positions is $3.87(2)^+$. This average value corresponds to 87% Mn^{4+} and 13% Mn^{3+}.

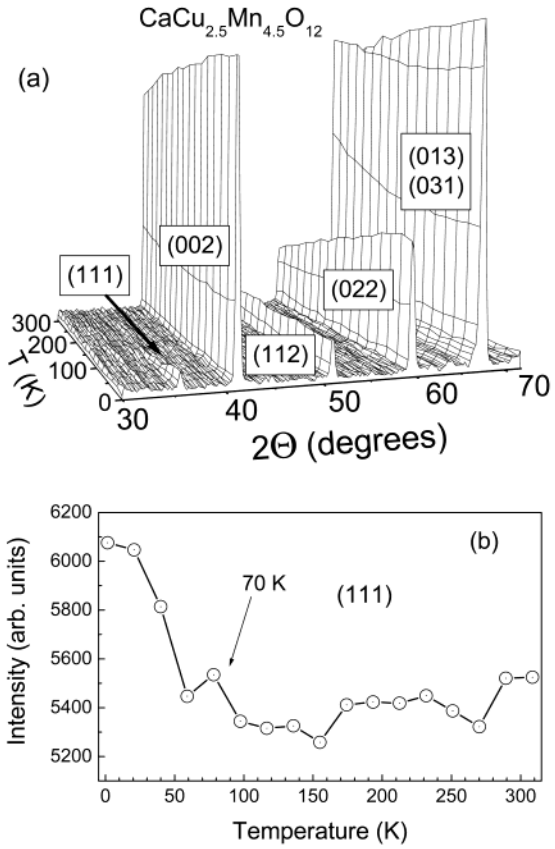

Figure 3. (a) Thermal evolution of the low-angle region of the NPD patterns of $CaCu_{2.5}Mn_{4.5}O_{12}$ collected at D1B−ILL diffractometer. (b) Temperature dependence of the intensity of the (1 1 1) reflection.

Magnetic Structure. Figure 3a shows the thermal evolution of the NPD patterns of $CaCu_{2.5}Mn_{4.5}O_{12}$ in the 1.5−312 K temperature range, collected in the high-flux D1B diffractometer. There is a magnetic contribution to the scattering on the low angle Bragg reflections, particularly visible on the [0 0 2] Bragg position, at $2\theta \approx 41°$. This contribution is characteristic of a ferromagnetic ordering, in which the magnetically ordered unit cell coincides with the crystallographic one. Additionally, an extra peak of magnetic origin appears below 70 K at the (1 1 1) Bragg position, forbidden by the body-centered unit cell but still indexable in a cubic unit cell of 7.22 Å edge. Figure 3b shows the thermal evolution of the (1 1 1) reflection. The presence of this peak suggests that the collinear arrangement of the magnetic moments in a perfect ferromagnet is lost, and there is an effect of canting of the magnetic moments. This implies the appearance of an additional antiferromagnetic component in the magnetic ordering, giving rise to magnetic neutron scattering in Bragg positions outside the crystallographic reflections, corresponding to an AFM superlattice.

To the best of our knowledge, the low-temperature magnetic structure of the parent $CaCu_3Mn_4O_{12}$ oxide

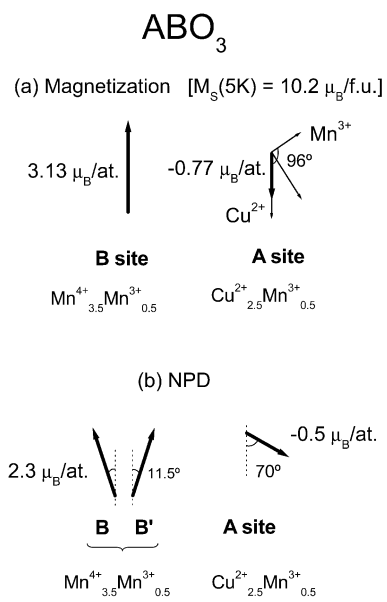

Figure 4. Schematic diagram showing (a) a model for the magnetic moments at the magnetic A sites and B sites of the ABO_3 perovskite, accounting for the observed saturation magnetization at 5 K; and (b) ordered magnetic moments at the A and B sites observed by NPD at 2 K.

has not been studied experimentally by neutron diffraction, although a ferrimagnetic structure, implying an antiferromagnetic coupling of the Mn and Cu magnetic moments, has been suggested from band structure calculations.[5] With this in mind, in a first trial we have modeled a perfect ferrimagnetic ordering between the magnetic moments at 6b and 8c positions, and refined this model for the 2 K D2B data of our material. After the full refinement of the profile, including the magnetic moments, a discrepancy R_{mag} factor of ~8% was reached. This trial model corresponds to a perfect collinear arrangement of Cu and Mn spins. The further introduction of a variable angle between two sets of Mn moments (those related by the body centering translation of $[^1/_2\ ^1/_2\ ^1/_2]$) allowed us to perfectly explain the magnetic contribution at the (1 1 1) forbidden position. The canting angle between the two nonequivalent Mn substructures is of 23°. A further degree of freedom was introduced by refining the relative angle between Mn at 8c and Cu(Mn) at 6b positions: the refinement finally led to ordered moments of 2.32(5) μ_B and −0.54(3) μ_B for 8c and 6b, respectively, oriented with a relative angle of 70°. The expected magnetic moment at the $Cu(Mn)_{6b}$ site, considering a parallel orientation of the Cu^{2+} and Mn^{3+} moments, would be of 1.5 μ_B/at. Our results seem to indicate that (i) the Cu(Mn) moments at 6b are not fully ordered, or Cu^{2+} and Mn^{3+} moments are not arranged in-phase, and (ii) the global magnetic moment at 6b positions is not ferrimagnetically (antiparallel) ordered with respect to the Mn moments at 8c. Figure 4 depicts a schematic model on the relative arrangement of the magnetic moments at both substructures. These results will be further discussed in light of the magnetization measurements. It is important to underline that, although neutron powder diffraction techniques do not allow determination of the absolute orientation of the magnetic moments in a cubic structure, it is indeed possible to determine the relative orientation of the moments of two different magnetic substructures.

Table 1. Unit-Cell, Positional, and Thermal Parameters, and Ordered Magnetic Moments for $CaCu_{2.5}Mn_{4.5}O_{12}$ in Cubic $Im\bar{3}$ (No. 204) Space Group, $Z = 2$, from NPD Data at 295 and 2 K[a]

	295 K	2 K
a (Å)	7.22793(5)	7.21901(5)
V (Å^3)	377.608(5)	376.212(5)
Ca	2a (0 0 0)	
B (Å^2)	0.67(7)	0.50(7)
(Cu,Mn2)	6b ($0\ ^1/_2\ ^1/_2$)	
B (Å^2)	0.39(4)	0.13(4)
f_{occ}(Cu)	0.808(8)	0.808(8)
magn. mom. (μ_B)	−0.21(9)	−0.54(3)
Mn1	8c ($^1/_4\ ^1/_4\ ^1/_4$)	
B (Å^2)	0.41(3)	0.39(3)
magn. mom. (μ_B)	1.10(5)	2.32(5)
O	24g (0 y z)	
y	0.3030(1)	0.3031(1)
z	0.1823(1)	0.1820(1)
B (Å^2)	0.55(1)	0.48(1)
reliability factors		
χ^2	1.92	7.02
R_p (%)	4.15	4.05
R_{wp} (%)	5.59	5.66
R_I (%)	3.73	6.15
R_{mag} (%)	3.72	8.16

[a] Reliability factors for both patterns are also given.

In this case we have considered that the first set of Mn^{4+} moments at 8c positions is parallel to the c-axis, and then refined the position of the second Mn^{4+} set and (Cu, Mn) moments at 6b with respect to this reference.

Refinement of the RT high-resolution data was completed after the introduction of the magnetic contribution arising from both 6b and 8c atomic positions, nonnegligible at RT, as shown from the magnetic measurements (Figure 2). The magnitude of the ordered magnetic moments at RT was 1.10(5) and −0.21(9) μ_B for 8c and 6b positions, respectively. In this case we considered a perfect antiferromagnetic arrangement between the two substructures because no pure magnetic reflections are observed outside the crystallographic Bragg 2θ positions at RT. Table 1 includes the unit-cell, atomic and thermal parameters, and discrepancy factors. Figure 5 shows the agreement between observed and calculated NPD profiles at RT and 2 K. Table 2 contains a list of selected bond distances and angles.

Magnetotransport Measurements. The transport properties of $CaCu_{2.5}Mn_{4.5}O_{12}$ are illustrated in Figure 6. Both $\rho(\boldsymbol{H} = 0)$ and $\rho(\boldsymbol{H} = 9\ T)$ curves show a broad maximum centered at 183 K ($\boldsymbol{H} = 0$) and 220 K ($\boldsymbol{H} = 9$ T). It is worth mentioning that the observed value for $\rho(T = 300\ K, \boldsymbol{H} = 0)$, of 0.093 Ω·cm, is considerably smaller than that described for the parent $CaCu_3Mn_4O_{12}$ compound,[3] of ~1.8×10^3 Ω cm. In a previous work, $\rho(T = 300\ K, \boldsymbol{H} = 0)$ is significantly lower, of 0.054 Ω·cm. In both cases, the low resistivity value suggests an increase of the carrier density with respect to the parent compound, probably related to the mixed valence state induced on the Mn cations at B positions of the perovskite. Figure 7 depicts the thermal evolution of the Seebeck coefficient in the temperature range 2 to 400 K. The negative slope indicates n-type behavior. The linear behavior indicates a metallic character, with a smooth change of slope after 200 K. No special anomaly is observed around T_C. Regarding the changes in $\rho(T)$

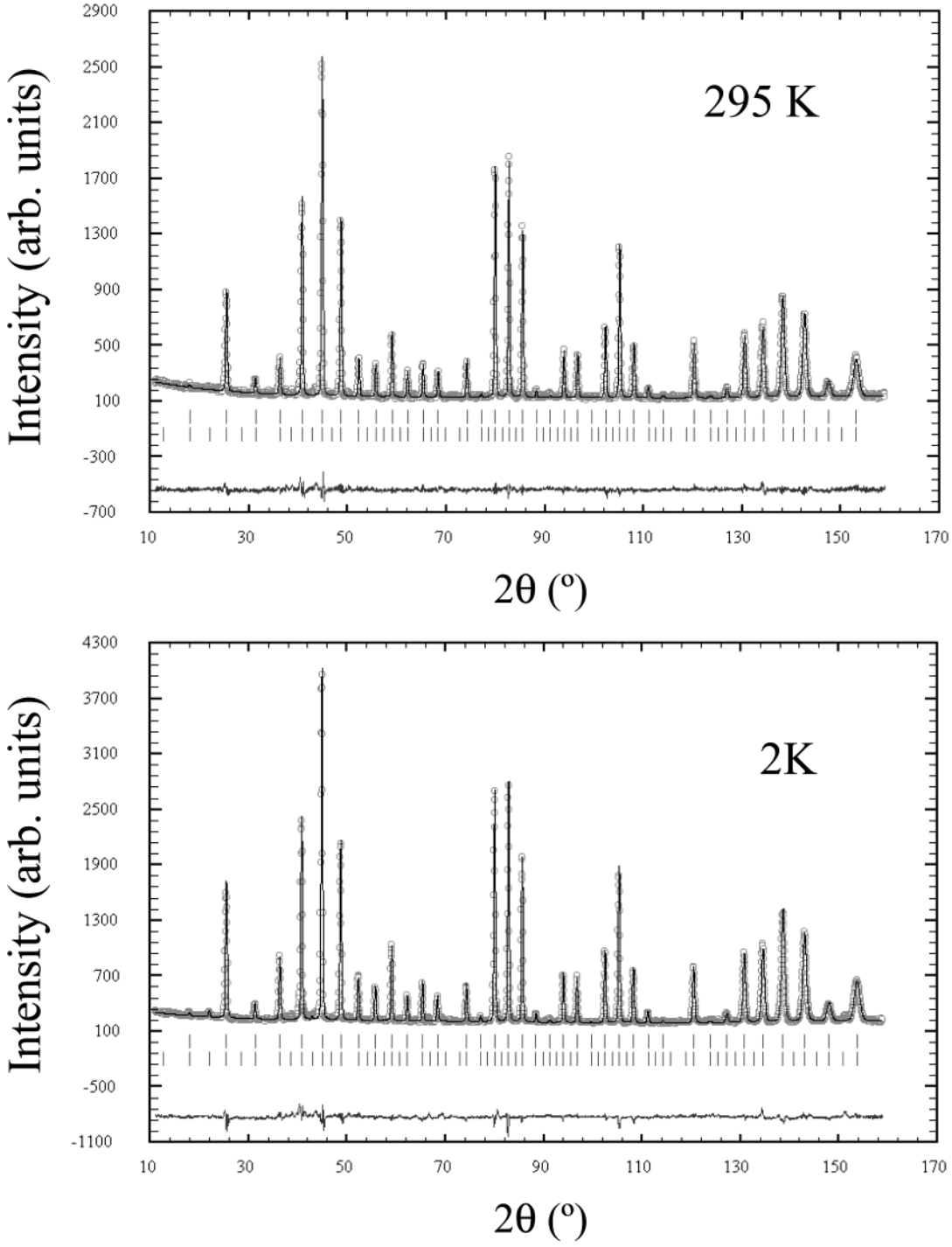

Figure 5. Observed (crosses), calculated (full line), and difference (bottom) NPD Rietveld profiles for $CaCu_{2.5}Mn_{4.5}O_{12}$ at 295 and 2 K, collected at the high-resolution D2B−ILL diffractometer. The second row of tick marks corresponds, in both spectra, to the magnetic structure.

under a magnetic field we define MR($\boldsymbol{H}$) = 100 × [R($\boldsymbol{H}$) − R(0)]/R(0). Figure 8 shows the thermal variation of MR with $\boldsymbol{H}$ = 9 T. The magnetoresistance is negative and increases (in absolute value) with decreasing temperature, reaching a maximum value of −34% at 5 K and 9 T. There is no apparent relationship between MR and T_C, which suggests that MR has an extrinsic origin. This point will be discussed later. The evolution of MR versus the magnetic field is shown in Figure 9 as isotherms at selected temperatures in the $\boldsymbol{H}$ = 0−9 T range. MR is still significant at RT, displaying values close to 7% for $\boldsymbol{H}$ = 9 T. The most striking feature of these isotherms is the strong component of low-field MR, defined for magnetic fields lower than 1 T. A value of MR(1 T) higher than 25% is observed at 2 K, and it is not negligible (about 2%) at RT. These figures make this compound a candidate for applications in spin-tronics devices.

Discussion

The cubic perovskite superstructure of $CaCu_{2.5}Mn_{4.5}O_{12}$ contains several features that must be highlighted. Ca atoms are coordinated to 12 oxygen atoms,

Table 2. Main Bond Distances (Å) and Selected Angles (°) for $CaCu_{2.5}Mn_{4.5}O_{12}$ Determined from NPD Data at 295 and 2 K

		295 K	2 K
CaO_{12} polyhedra			
Ca−	O (×12)	2.5558(7)	2.5521(7)
CuO_{12} polyhedra			
Cu−	O (×4)	2.7023(9)	2.7002(5)
Cu−	O (×4)	3.1738(6)	3.1713(7)
Cu−	O (×4)	1.9395(6)	1.9357(9)
O−Cu−O[a]		94.45	94.51(7)
O−Cu−O[a]		85.55	85.49(7)
MnO_6 octahedra			
Mn−	O (×6)	1.9110(7)	1.9092(7)
O−Mn−O		89.93(7)	89.90(6)
O−Mn−O		90.08(4)	90.10(7)
Cu−O−Mn		108.74(3)	108.78(3)
Mn−O−Mn		142.01(1)	141.93(1)

[a] For Cu−O short distances, within CuO_4 square units.

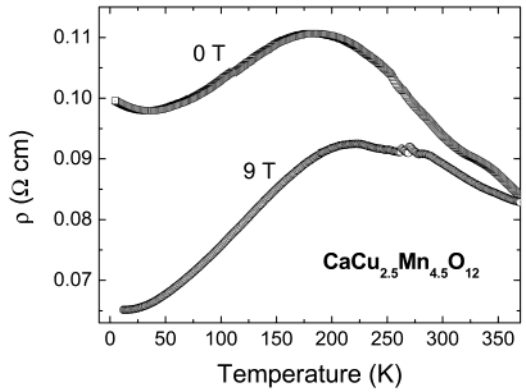

Figure 6. Resistivity vs temperature curves at $\boldsymbol{H} = 0$ and 9 T.

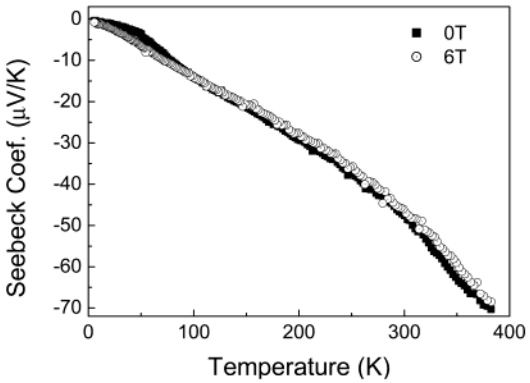

Figure 7. Thermal variation of the Seebeck coefficient at $\boldsymbol{H} = 0$ and 6 T for $CaCu_{2.5}Mn_{4.5}O_{12}$.

with equal Ca−O distances, whereas the oxygen environment for (Cu^{2+}, Mn^{3+}) cations is highly irregular, with 8 rather long distances (2.70 and 3.17 Å at RT) and an effective coordination number of four, with Cu−O bond lengths of 1.94 Å at RT in a pseudo-square arrangement (Table 2). These CuO_4 units are not strictly coplanar, exhibiting O−Cu−O angles of 94.5° and 85.5°. At the B substructure of the perovskite, (Mn^{4+}, Mn^{3+}) cations occupy the center of virtually regular octahedra, with Mn−O bond lengths of 1.91 Å at RT. The actual oxidation states of the different cations present in the solid can be assessed by means of the Brown's bond

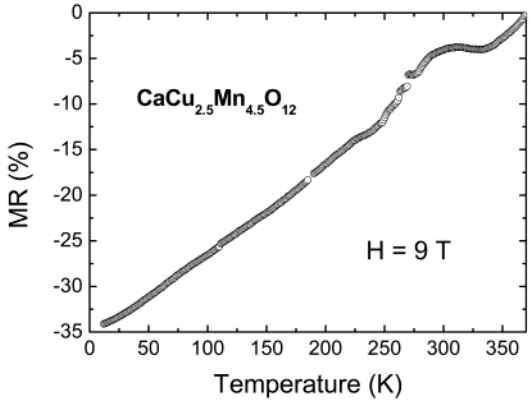

Figure 8. Temperature dependence of the magnetoresistance at 9 T, defined as $100 \times [R(0) - R(9\ \mathrm{T})]/R(0)$.

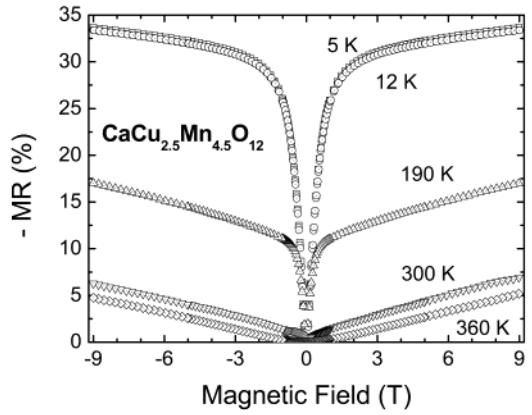

Figure 9. Magnetoresistance (MR) isotherms for $CaCu_{2.5}Mn_{4.5}O_{12}$. MR is defined as $100 \times [R(0) - R(9\ \mathrm{T})]/R(0)$.

valence theory,[13,14] from the observed metal−oxygen distances. This theory gives a phenomenological relationship between the formal valence of a bond and the corresponding bond length. In perfect nonstrained structures the bond valence sum (BVS) rule states that the formal charge of the cation (anion) is equal to the sum of the bond valences around this cation (anion). This rule is satisfied only if the stress introduced by the coexistence of different structural units can be relieved by the existence of enough degrees of freedom in the crystallographic structure. The departure of the BVS rule is a measurement of the existing stress in the bonds of the structure.

From the distances listed in Table 2, we obtain valences at RT of 2.40, 1.94, and 3.84 for Ca, (Cu,Mn) at 6b, and Mn at 8c positions, respectively. The valence of Ca cation is slightly higher than the expected value of 2+; this result suggests that Ca atoms are overbonded and under compressive stress in the crystal, giving rise to a structure with a significant metastable character: this is related to the requirement of a high-pressure synthesis. The slight deviation from the divalent Cu valence can be understood by the presence at the same crystallographic sites of high-spin Mn^{3+}, with a larger ionic radius, accounting for overall (Cu,Mn)−O distances slightly larger than those expected for Cu−O. The

(13) Brown, I. D. In *Structure and Bonding in Crystals;* O'Keefe, M., Navrotsky,A., Eds.; Academic Press: New York, 1981; Vol. 2, pp 1−30.

(14) Brese, N. E.; O'Keefe, M. *Acta Crystallogr. Sect. B* **1991**, *47*, 192.

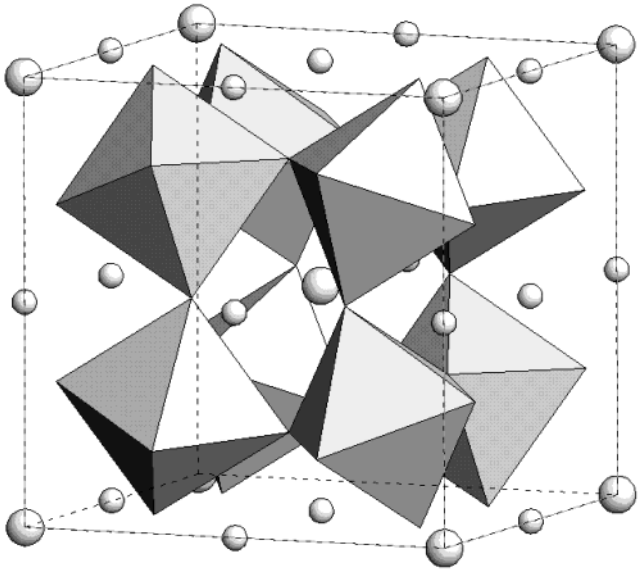

Figure 10. View of the structure of $CaCu_{2.5}Mn_{4.5}O_{12}$: *c* axis is vertical; *a* axis from right to left. Large and small spheres represent Ca and Cu, respectively; corner-sharing MnO_6 octahedra are fairly tilted in the structure to optimize Ca−O and Cu−O bond lengths.

valence for Mn at 8c (octahedral environment) is lower than 4+, and very close to the nominal valence of 3.875+ for the $CaCu_{2.5}Mn_{4.5}O_{12}$ composition.

A view of the crystal structure of $CaCu_{2.5}Mn_{4.5}O_{12}$ is shown in Figure 10. It is fairly distorted due to the small size of Ca^{2+} and Cu^{2+}cations, which force the MnO_6 octahedra to tilt in order to optimize the Ca−O bond distances. The tilting angle of the octahedra can be simply derived from the Mn−O−Mn angle, to be 19° at RT.

The ordered magnetic moment found from NPD data at Mn (octahedral, 8c) positions, of 2.32(5) μ_B at 2 K, is slightly lower than expected for ($Mn_{3.5}^{4+}Mn_{0.5}^{3}$) of 3.12 μ_B per atom, suggesting some electronic delocalization due to covalent effects. The fact that a canting angle between the Mn_{8c} moments appears below a certain temperature can be accounted for by considering that the Mn−O−Mn bond angle in $CaCu_{2.5}Mn_{4.5}O_{12}$ is ∼142°, at halfway between 180°, for which an AFM interaction between Mn magnetic moments is expected, and 90°, for which a FM is predicted from the Goodenough−Kanamori rules.[15] The presence of canting involves both FM and AFM interactions.

For a perfect ferrimagnetic arrangement of the A and B substructures the expected saturation magnetic moment would be 8μ_B/fu, for the stoichiometry $Ca^{2+}(Cu_{2.5}^{2+}Mn_{0.5}^{3+})_A(Mn_{3.5}^{4+}Mn_{0.5}^{3+})_BO_{12}$ (Cu^{2+}, $S = {}^1/_2$; Mn^{3+}, $S = 2$; Mn^{4+}, $S = {}^3/_2$). Figure 4a helps to illustrate the observed saturation magnetization at 5 K of 10.2 μ_B/fu. Our results can be explained in a model that considers that $(Mn_{3.5}^{4+}Mn_{0.5}^{3+})_B$ moments are ferromagnetically coupled, and antiferromagnetically coupled to Cu^{2+} moments at A sites. At the A sites, the Cu^{2+} and Mn^{3+} moments are canted, giving a FM projection with respect to the B substructure (see Figure 4a). To obtain the observed magnetization, Cu^{2+} and Mn^{3+} moments are disposed with an angle of about $\theta = 96°$, in such a way that the net magnetization moment at this site is 0.77 μ_B/atom, in excellent agreement with the magnetic moment determined by NPD at this position (Figure 4b).

The magnitude of the resistivity of our sample is almost twice that reported for $CaCu_{2.5}Mn_{4.5}O_{12}$ by Zeng et al.,[10] also showing a semiconductor-to-metal transition around 180 K. We think this difference could be due to the more perfect oxygen stoichiometry of our sample, prepared under more strongly oxidizing conditions; slight oxygen deficiencies would increase the electron doping effect (lowering the valence of Mn cations at 8c positions), thus reducing the resistivity. Note that the parent compound, $CaCu_3Mn_4O_{12}$, displays a resistivity 4 orders of magnitude bigger, exhibiting a semiconducting behavior in the whole temperature range.[3] The MR observed at low temperature and 5 T is 33%; this is larger than that reported in ref 10 (28%), which can be correlated with the higher value of the resistivity, and presumably a lower number of carriers than the sample of ref 10. In $CaCu_3Mn_4O_{12}$ compound, MR is around 40%. The MR is always negative and increases with decreasing temperature (Figure 8). The fact that MR in these materials is not related to the Curie temperature, T_C, suggests a mechanism of spin polarized inter-grain tunneling.[16,17] It has been reported that in the $CaCu_{3-x}Mn_{4+x}O_{12}$ series the MR diminishes when the amount of Mn^{3+} at the 6b positions increases, as a result of the increment in the net number of carriers in the system. Recently, Majumdar and Littlewood[18] demonstrated that there is a relationship between the MR and the reciprocal of the charge carrier density (n), according to the equation $MR = C(M/M_s)^2$, where M_s is the saturation magnetization and C is proportional to $n^{-2/3}$. One of our main findings is that, despite the presence of some Mn^{3+} at the Cu^{2+} sites, which is inherent to the moderate-pressure preparation conditions, we have obtained MR ratios similar to those described for the term of the series, $CaCu_3Mn_4O_{12}$. Moreover, we have shown that MR shows a very good response at low field, even at RT, comparable to the best results reported for manganese perovskites.

Regarding the origin of the upturn observed in the resistivity at around 70 K, where the material becomes semiconducting (Figure 6), we think it can be ascribed to the presence of additional magnetic scattering of the charge carriers, as it seems to be strongly correlated to the anomaly observed in the ZFC susceptibility at about the same temperature. This effect corresponds to the appearance of a canting effect in the ordered magnetic moments, as revealed in the NPD experiments. In fact, the low-temperature semiconducting behavior almost vanishes when applying a magnetic field of 9 T (Figure 6), as it does the magnetic anomaly in the FC susceptibility curve.

Conclusions

Single phase $Ca^{2+}(Cu_{2.5}^{2+}Mn_{0.5}^{3+})Mn_4^{3.875+}O_{12}$ with a perovskite-related structure was synthesized at a mod-

(15) Goodenough, J. B. *Magnetism and the Chemical Bond*; Interscience Publishers: New York, 1963.

(16) Hwang, H. Y.; Cheong, S.-W.; Ong, N. P.; Batlogg, B. *Phys. Rev. Lett.* **1996**, *77*, 2041.

(17) Kobayashi, K.-I.; Kimura, T.; Sawada, H.; Terakura, K.; Tokura, Y. *Nature* **1998**, *395*, 677.

(18) Majumdar, P.; Littlewood, P. *Nature* **1998**, *395*, 479.

erate pressure of 20 kbar in the presence of an oxidizing agent. The structural refinement from RT and 2 K high-resolution NPD data was performed in order to unravel the microscopic origin of the magnetic and magnetotransport behavior in this material. We have found that the 6b positions of the perovskite are randomly occupied by Cu^{2+} and Mn^{3+} cations; both magnetization and NPD measurements suggests that their magnetic moments are not aligned but present a canting angle of about 96°, despite occupying the same crystallographic positions. Below a characteristic temperature of 70 K, there is an additional canting of the Mn moments at the 8c positions, leading to a loss of the body-centered symmetry and the appearance of a low-angle superstructure peak. This canting promotes the magnetic scattering of the charge carriers and is at the origin of the observed low-temperature semiconducting behavior. The resistivity and MR of our material are superior to those described for samples prepared under softer conditions; moreover the MR is comparable to that exhibited by $CaCu_3Mn_4O_{12}$, which requires much higher pressures to be stabilized. This is probably due to the full oxygen stoichiometry exhibited by our sample, as verified by neutron diffraction. Finally, the high sensitivity of MR at low fields and its temperature stability make this material a good candidate for future technological applications.

Acknowledgment. We thank CICyT for financial support of the project MAT 2001-0539, MAT2002-1329, and MAT2000-1384, and we are grateful to ILL for making all facilities available.

CM0212616